Adsorption, 1, 213–231 (1995)

Adsorptive Separation by Thermal Parametric Pumping Part I: Modeling and Simulation

LICÍNIO M. FERREIRA* AND ALÍRIO E. RODRIGUES
Lab. of Separation and Reaction Engineering, School of Engineering, University of Porto, 4099 Porto Codex, Portugal

Abstract. A detailed model for the recuperative parametric pumping is presented. The model includes intraparticle mass transfer resistance, axial diffusion and non-linear equilibrium represented by Langmuir equation. The sensitivity studies shows that process performance strongly increases when cycle time increases and ϕ_B/ϕ_T ratio and particle size decreases. It also shows that bottom and top dead volumes do not influence much the process performance. Evolution of the histories of concentrations and temperatures, the bed performance from cycle to cycle and the bed dynamics at the cyclic steady state have been discussed.

The model revealed itself as useful to simulate the behavior of the recuperative parametric pumping process and was applied to predict optimal experimental results for the system phenol-water/Duolite ES-861 (Part II).

Keywords: adsorptive separation, thermal parametric pumping, modeling, simulation

Introduction

Parametric pumping is a dynamic separation process based on the differences in the adsorption equilibrium caused by a cyclic change of a thermodynamic variable (temperature, pressure, pH). In thermal parametric pumping the adsorbent is in a fixed bed column and when the temperature changes the flow is reversed, i.e., the fluid mixture moves upward at hot temperature and downward at cold temperature. Since the solid phase can adsorb less solute at the hot temperature than at the cold temperature, we would expect the adsorbed phase concentration to increase when temperature decreases.

There are two ways to operate a thermal parapump process: the direct mode and the recuperative mode. In the direct mode the temperature change is imposed through the column wall, whilst in the recuperative mode the fluid mixture entering into the column is heated or cooled.

A closed system parapump has no feed or product streams and a open system requires a feed reservoir and two reservoirs to collect the top and the bottom products. In an open system operating in recuperative mode the enrichment of the solute occurs in the top reservoir whilst an almost free-solute solution is obtained in the bottom reservoir, under appropriate conditions.

*Present address: Chemical Engineering Department, University of Coimbra, 3000 Coimbra, Portugal.

The technique of separation by parametric pumping is an alternative to conventional adsorption process and presents some advantages. The major difference between the two operations is the following: in conventional adsorption the solution is percolated in a single direction until the column is saturated and the column is then regenerated; in parametric pumping the process evolution is made by successive cyclic changes in flow direction coupled with changes in the thermodynamic variable, such as temperature. The column is never completely saturated or regenerated. In general, chemical regenerant is never needed by thermal parapump systems; the bed is regenerated with low potential thermal energy.

This stimulates the commercial interest in using the operation as a solvent purification or solute concentration technique. Parametric pumping can be also useful for protein separations on ion-exchange columns. Since the net charge on a protein is dependent on pH, periodic variations of that variable accompanied with the change in the flow direction makes the separation possible. Several pH parapump devices were used by Chen et al. (1977, 1979 and 1980) for separating hemoglobin and albumin on CM Sepharose. Holl et al. (1982) demonstrated that the protein separations can be improved by applying an electrical field in addition to the pH.

Several models have been presented to describe open and closed thermal parametric pumping. All of them

can be classified as follows: complete models and equilibrium models. The first group takes into account dispersive effects (mass transfer resistances and axial dispersion) and in the second those effects are neglected. The complete models consist of parabolic partial differential equations (PDE) which are solved numerically. Equilibrium models lead to hyperbolic PDE's which can be solved analytically by the method of characteristics. A rapid ideal solution is obtained by solving the equilibrium model allowing us to get a useful insight into the parametric pumping separation.

The equilibrium theory was first used by Pigford et al. (1969), and assumes linear isotherms, local equilibrium between the solid and the liquid phases, constant fluid velocity and no axial dispersion. Gregory and Sweed (1970) applied the theory to various configurations and operations of open systems; Chen and Hill (1971), Chen et al. (1972, 1973) treated continuous systems. Equilibrium model solutions for non mixed dead volumes were presented by Costa et al. (1982). A complete model, first stated by Wilhelm et al. (1966), included non-linear isotherm, mass transfer resistance concentrated in the interphase liquid/solid and no axial dispersion. A more complete model, including axial dispersion, was considered by Wilhelm et al. (1968). Sweed and Wilhelm (1969) used a model without axial dispersion and an interphase transfer rate relationship for the direct thermal mode; experimental separations were simulated with the STOP-GO algorithm (a modification of the method of characteristics). This algorithm was also applied to closed systems by Sweed and Gregory (1971). Other workers have modeled the adsorption process in parametric pumping. Gupta and Sweed (1973), approached the fixed bed with the mixing cell model. A stage equilibrium theory was employed by Wankat (1973) to describe the liquid-liquid extraction parametric pumping. The stage theory was also utilized by Grevillot and Tondeur (1976, 1977) and Grevillot (1980) by analyzing the analogy between parametric pumping and distillation. A near-equilibrium approach with chemical reaction was used by Apostolopoulos (1975 and 1976) considering the parametric pumping system as a chemical reactor. Foo and Rice (1975 and 1977) and Rice (1976) studied the effect of radial heat transfer over the ultimate separation using frequency response solutions.

Complete models reported in the literature always consider a lumped parameter representation of interphase solute mass transfer. This assumption is valid when intraparticle gradients are negligible. This paper presents a more detailed model, for the recuperative mode, in which the intraparticle mass transfer resistance is taken into account.

The objectives of this work are:

i) to study the effect of operating variables on the process performance;
ii) to analyze the evolution of the concentration and temperature histories and axial profiles from the start-up of the parametric pump until the cyclic steady state;
iii) to understand the process dynamics at the cyclic steady state.

Process Description

The process modeled is a semicontinuous process, with feed at the top reservoir, as is shown in Fig. 1. Each run is a series of cycles in which we have a hot half cycle followed by a cold half cycle. A typical cycle starts with the column in equilibrium with feed solution at the hot temperature and the bottom reservoir containing this fluid. In the hot half cycle the liquid solution flows from the bottom reservoir into the top reservoir. In the cold half cycle the liquid solution flows from

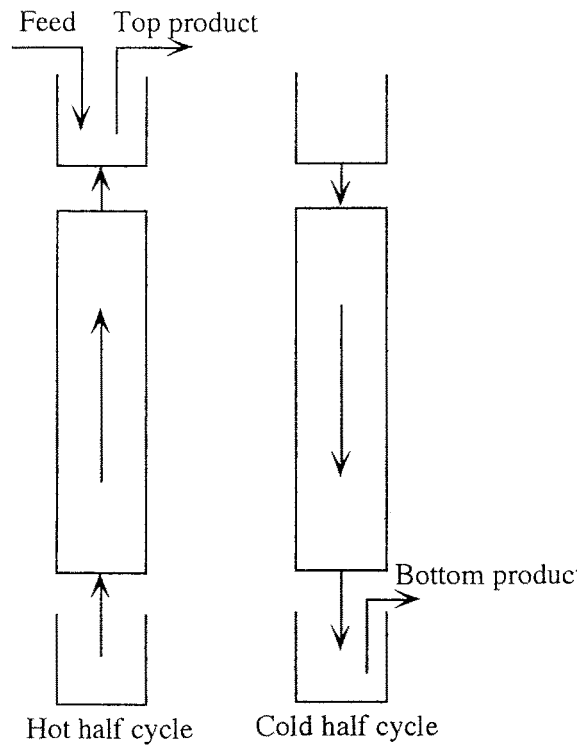

Fig. 1. Semicontinuous top feed parametric pumping.

the top reservoir into the bottom reservoir. The top product is withdrawn and feed is added during the hot half cycle and the bottom product is withdrawn during the cold half cycle. Temperatures at the column ends were 60°C (bottom) and 20°C (top). The end of each half cycle was determined by the time at which all the solution contained in a reservoir was transferred, either downward or upward.

Mathematical Model

The model is based on the equations used for adsorption systems in fixed bed and includes mass and heat balances in a volume element of the column for each phase, non-linear adsorption equilibrium between fluid and adsorbed phase inside particles and boundary and initial conditions. Since the system is open, we must include external balances to consider the effects of feed, products and reflux from the reservoirs. The flow pattern in described by axial dispersed plug flow. The intraparticle mass transfer is described by a pore-diffusion model and the film mass transfer was also considered.

In addition, we assume:

- A one-dimensional pseudo homogeneous model for the heat transfer.
- Constant physical properties of the fluid and the solid.
- Negligible effect of the transient temperature regimen on the mass and heat transfer parameters.
- The adsorption equilibrium is described by a Langmuir isotherm ($q^* = \frac{K_L Q_\infty C^*}{1+K_L C^*}$); the equilibrium constant obeys to the normal exponential temperature dependence, that is, $K_L = k_0 e^{-\Delta H/RT}$, where $(-\Delta H)$ is the heat of adsorption and k_0 is constant.
- Mixed reservoirs.

The dimensionless model equations can be summarized, as follows,

Mass balance in a volume element of the column:

$$\frac{1}{\mathrm{Pe}}\frac{\partial^2 X(z^*,\theta)}{\partial z^{*2}} \pm \frac{\partial X(z^*,\theta)}{\partial z^*} = \frac{\partial X(z^*,\theta)}{\partial \theta} + N_f[X(z^*,\theta) - X_p(1,z^*,\theta)] \quad (1)$$

where $X = C/C_E$ and $X_p = C_p/C_E$ are the reduced concentrations in the bulk fluid and inside pores; $z^* = z/L$ is the reduced axial coordinate and $\theta = t/\tau$ ($\tau = \varepsilon L/u$) is the reduced time.

Energy balance in the column:

$$\frac{1}{\mathrm{Pe}_h}\frac{\partial^2 T^*(z^*,\theta)}{\partial z^{*2}} \pm \frac{\partial T^*(z^*,\theta)}{\partial z^*} - N_{\mathrm{hw}} T^* = (1+\xi_h)\frac{\partial T^*(z^*,\theta)}{\partial \theta} \quad (2)$$

(+)—downward flow
(−)—upward flow

where $T^* = T - T_a$ (T_a is the ambient temperature).

Mass balance inside particles:

$$\rho_h f_H \frac{\partial q(u^*,z^*,\theta)}{\partial \theta} + \varepsilon_p C_E \frac{\partial X_p(u^*,z^*,\theta)}{\partial \theta} = \varepsilon_p N_D C_E \left\{ \frac{2}{u^*}\frac{\partial X_p(u^*,z^*,\theta)}{\partial u^*} + \frac{\partial^2 X_p(u^*,z^*,\theta)}{\partial u^{*2}} \right\} \quad (3)$$

where q and C_E are the adsorbed phase and initial (feed) solute concentrations, respectively; $u^* = r/R_0$ is the reduced radial coordinate; ε_p, f_H and ρ_h are the intraparticle porosity, the humidity factor (Kg dry resin/Kg wet resin) and the wet density of the adsorbent, respectively.

Adsorption equilibrium isotherm:

$$q(u^*,z^*,\theta) = \frac{K_L Q_\infty C_E X_p(u^*,z^*,\theta)}{1 + K_L C_E X_p(u^*,z^*,\theta)} \quad (4)$$

$$K_L = k_0 \exp\left[\frac{(-\Delta H)}{R(T^* + T_a)}\right] \quad (5)$$

where K_L and Q_∞ are the parameters of Langmuir equilibrium relation; R is the ideal gas constant.

External balances (reservoirs):

Hot half cycle

$$\langle X_{\mathrm{BP}}\rangle_n = \langle X_{\mathrm{BP}}\rangle_{n-1} \quad (6)$$

$$\langle X_{\mathrm{TP}}\rangle_n = \frac{(1-\phi_B)\left\{\frac{(1-\phi_B)\langle X(1,\theta)\rangle_n + m_1\langle X(1,\theta)\rangle_{n-1}}{1+m_1-\phi_B}\right\}}{(1+\phi_T)} + \frac{(\phi_B+\phi_T)}{(1+\phi_T)} \quad (7)$$

Cold half cycle

$$\langle X_{\mathrm{BP}}\rangle_n = \frac{(1+\phi_B)\langle X(0,\theta)\rangle_n + m_2\langle X_{\mathrm{BP}}\rangle_{n-1}}{1+m_2+\phi_B} \quad (8)$$

$\langle X(1,\theta)\rangle_n$ and $\langle X(0,\theta)\rangle_n$ are the average of the exiting concentrations in top during the n-th hot half cycle and in bottom during the n-th cold half cycle, respectively; $\langle X_{\mathrm{BP}}\rangle_n$ and $\langle X_{\mathrm{TP}}\rangle_n$ are concentrations entering in the bottom during the n-th hot half cycle and in the top during the n-th cold half cycle, respectively. ϕ_B and

ϕ_T are the fractions of $Q(\pi/\omega)$ (reservoir displacement volume = fictitious flowrate in batch system (Q) x half cycle duration (π/ω), where ω is the pulsation) that are withdrawn as bottom and top products; and m_1 and m_2 are the dimensionless top and bottom dead volumes.

Boundary conditions:

Fluid

Upward flow (hot half cycle)

$z^* = 0$

$$X(0,\theta) = \langle X_{BP}\rangle_n; \quad T^* = T_{\text{hot feed}} - T_a \tag{9}$$

$z^* = 1$

$$\frac{\partial X(z^*,\theta)}{\partial z^*} = 0; \quad \frac{\partial T^*(z^*,\theta)}{\partial z^*} = 0 \tag{10}$$

Note that $z^* = 0$ is the bottom of the column and $z^* = 1$ is the top of the bed.

Downward flow (cold half cycle)

$z^* = 0$

$$\frac{\partial X(z^*,\theta)}{\partial z^*} = 0; \quad \frac{\partial T^*(z^*,\theta)}{\partial z^*} = 0 \tag{11}$$

$z^* = 1$

$$X(1,\theta) = \langle X_{TP}\rangle_n; \quad T^* = T_{\text{cold feed}} - T_a \tag{12}$$

Particle

$u^* = 0$

$$\left.\frac{\partial X_p(u^*,z^*,\theta)}{\partial u^*}\right|_{u^*=0} = 0 \tag{13}$$

$u^* = 1$

$$\varepsilon_p N_D \left.\frac{\partial X_p(u^*,z^*,\theta)}{\partial u^*}\right|_{u^*=1} = N_f \frac{\varepsilon}{1-\varepsilon}[X(z^*,\theta) - X_p(1,z^*,\theta)] \tag{14}$$

where ε is the bed porosity.

Initial conditions:

$\theta = 0$

$$X(z^*,0) = X_p(u^*,z^*,0) = 1 \quad (z^* > 0) \tag{15}$$

$$T^*(z^*,0) = T_0^*(z^*) - T_a \tag{16}$$

The model parameters are:

K_L and Q_∞: equilibrium adsorption isotherm parameters;

Pe $= \frac{uL}{\varepsilon D_{ax}}$: mass Peclet number;

$\text{Pe}_h = \frac{G_f c_{pf} L}{K_{ae}}$: heat Peclet number;

$N_D = \frac{\tau D_P}{R_0^2}$: number of intraparticle mass transfer units;

$N_f = \frac{3(1-\varepsilon)k_f\tau}{\varepsilon R_0}$: number of film mass transfer units;

$N_{hw} = \frac{h_{we}a_w\tau}{\rho_f c_{pf}\varepsilon}$: number of wall heat transfer units;

$\xi_h = \frac{(1-\varepsilon)\rho_s c_s}{\varepsilon\rho_f c_{pf}}$: thermal capacity parameter.

The film mass transfer coefficient k_f is calculated from the correlation $j_D = 7.32\ \text{Re}'^{-0.569}$ (Costa and Rodrigues, 1985), where $j_D = \text{Sh/Re Sc}^{1/3}$, $\text{Re}' = \text{Re}/(1-\varepsilon)$, $\text{Re} = ud_p/\nu$, $\text{Sc} = \nu/D_m$ and $\text{Sh} = k_f d_p/D_m$.

Results and Discussion

Numerical Method

The equations presented above lead to a system of parabolic, partial differential equations, in two spatial dimensions u^* and z^* and in time θ. The solution of model equations was carried out by numerical integration using a computer software package—PDECOL (Madsen, 1979), based on finite element collocation. That package only solves systems of nonlinear PDE's in one space and one time dimensions. It was therefore necessary to discretize the interval of the radial particle coordinate u^* by dividing it into NE subintervals. An approximate solution on each subinterval k can be represented by (Finlayson, 1980),

$$S(g_k, z^*, \theta) = \sum_{i=1}^{4} a_i(z^*,\theta)H_i(g_k) \tag{17}$$

where $H(g)$ are cubic Hermite polynomials, a_i are coefficients to be determined and g_k is the normalized radial coordinate for the subinterval k,

$$g_k = \frac{u^* - u_k^*}{h_k} \quad \text{with} \quad h_k = u_{k+1}^* - u_k^* \tag{18}$$

This methodology allowed us to transform the original system into (2NE + 2) one space dimension PDE's; 19 subintervals in the axial direction and 10 subintervals in the particle radial direction (NE) were used in the numerical solution by computer.

The values of parameters used in the simulations are shown in Table 1 concerning the experimental system phenol-water/Duolite ES-861 (Ferreira, 1994).

Table 1. Parameter values used in the simulations of the recuperative parametric pumping (semicontinuous process).

Resin characteristics	Bed characteristics
ρ_h (kg wet resin /m^3 wet resin) = 1020	$L(m) = 0.75, 0.85$
f_H (kg dry resin /kg wet resin) = 0.28	$d(m) = 0.09$
$R_0 \times 10^4$(m) = 1, 1.5, 2, 2.35*, 3	$\varepsilon = 0.4$
$\varepsilon_p = 0.72$	
$\tau_p = 2.93$	Transport parameters
$\xi_h = 1.3$	D_m (m^2/s) [20°C] = 8.9×10^{-10}
	D_m (m^2/s) [60°C] = 2.2×10^{-9}
Operating variables	h_{we} (kJ/m^2.K.s) = 1.42×10^{-2}
T_{hc} (K) = 333.15 (60°C)	
T_{cc} (K) = 293.15 (20°C)	Equilibrium parameters
T_a (K) = 297.15 (24°C)	Q_∞ (kg solute /kg dry resin)
V_U (m^3) = 0.0236	= 0.03, 0.05, 0.07*, 0.08
$Q[\pi/\omega]$ (m^3) = 0.0324	k_0 (m^3 solution /kg solute)
$\phi_B = 0.27$ and $\phi_t = 0.14$	= 3.96×10^{-4}
$m_1 = 0^*, 0.1, 0.3$ and $m_2 = 0^*, 0.1, 0.3$	$[-\Delta H]$ (kJ/kmol) = 22751
$t_c(h) = 2.9, 3.5, 4, 5.6^*, 6.2$	
Model parameters	
Pe = 20, 50, 120*	
$\text{Pe}_h = 100$	

*Values used in all the simulations, where the effect of the corresponding parameter is not being studied.

Our goal is to explore the operating conditions that yield the best separation in terms of the solvent purification. The separation performance is defined here as the ratio between the species concentration in the top and bottom reservoir, respectively.

Sensitivity Studies

Computer simulations were carried out to understand how the separation performance is influenced by: a) the cycle time, t_c; b) the adsorbent particle size, R_0; c) the Peclet number, Pe; d) the dimensionless dead volumes, m_1 (top) and m_2 (bottom); e) the fraction of reservoir volume obtained as bottom product, ϕ_B; f) the adsorbent capacity, Q_∞ and g) the temperature change, ΔT.

Effect of the Cycle Time, t_c. Changes in the flowrate, either in upward flow or downward flow, affect directly the cycle time duration; the separation tends to improve at longer cycle times, i.e., when the flowrate decreases as shown in Fig. 2. This result may be understood by considering that at lower flowrate longer contact is established between the mobile phase and the adsorbent, making the operation closer to the equilibrium. On the other hand, if the cycle time is too long breakthrough can occur, meaning that some solute will pass through the column without undergoing a temperature change (ΔT).

In terms of heat transfer, an opposite effect is observed because better separation is obtained when the flowrate increases. During the hot half cycle, in upward flow, the stationary temperature at the top of the column increases at higher flowrate and will tend to the temperature of the feed solution, in the bottom of the column, at infinitely high flowrate. It follows that during the cold half cycle each section in the column will undergo higher temperature difference and more separation will occur.

Concerning the simulations displayed in Fig. 2, it can be seen that the influence of the cycle time (by changing the flowrate) on the separation is controlled by mass transfer limitations.

Table 2 shows how the model parameters for each simulation are changed when the cycle time takes different values. These values are obtained by changing the flowrate either in the hot half cycle (Q_{hc}) or the cold half cycle (Q_{cc}). Looking at the first row in Table 2 where a cycle time of 2.9 h is considered, the duration of the hot half cycle to percolate all the volume contained in the bottom reservoir $V_U = 0.0236$ m^3 at $Q_{hc} = 5 \times 10^{-6}$ m^3/s is $t_{hc} = 79$ min; N_D equals to 5.92

Table 2. Parameter values used in the simulations to study the effect of the cycle time.

$Q_{hc}10^6$ (m^3/s)	$Q_{cc}10^6$ (m^3/s)	t_{hc} (min)	t_{cc} (min)	t_c (h)	$N_{D(hc)}$	$N_{D(cc)}$	$N_{f(hc)}$	$N_{f(cc)}$	$N_{hw(hc)}$	$N_{hw(cc)}$
5.00	5.83	79	93	2.9	5.92	2.15	1125	466	0.16	0.14
4.42	4.17	89	130	3.5	6.70	3.02	1125	582	0.19	0.20
4.42	3.53	89	152	4.0	6.70	3.56	1125	641	0.19	0.23
2.50	5.83	157	217	6.2	11.83	5.03	1688	815	0.33	0.33

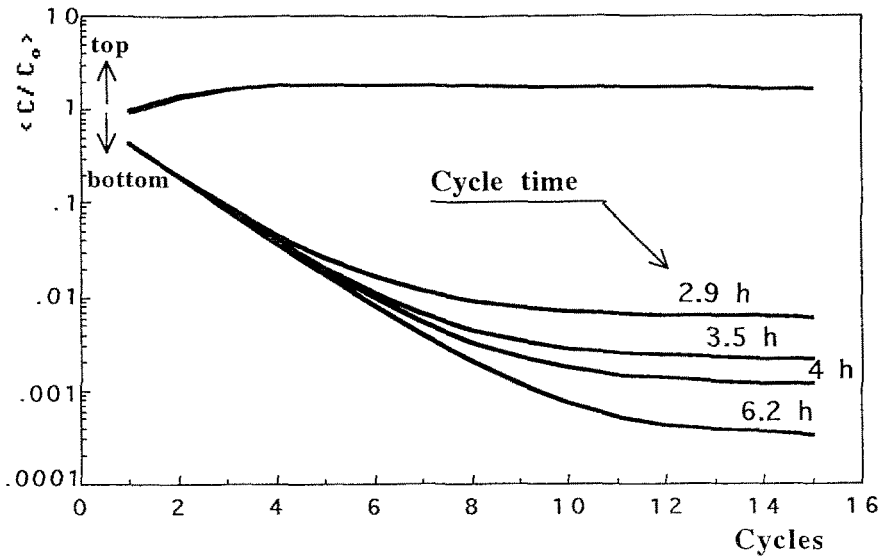

Fig. 2. Effect of the cycle time on top and bottom transient concentrations versus the number of cycles.

for that half cycle calculated with $D_p\ (=D_m/\tau_p) = 7.509\times10^{-10}\ m^2/s$, $R_0 = 2.35\times10^{-4}$ m and $\tau = 435$ s. Similarly, the duration of the cold half cycle t_{cc} needed to flow upwards 0.0324 m^3 at $Q_{cc} = 5.83\times10^{-6}\ m^3/s$ is 93 min.

Since the parameters vary directly with the space time in the column and so inversely with the velocity, we can conclude that N_D, N_f and N_{hw} values increase when the flowrate decreases.

Effect of the Adsorbent Particle Radius, R_0. Since the diffusion inside particles is the controlling step, better separation is obtained when smaller particles of the adsorbent is used. This effect is shown in Fig. 3. When R_0 decreases, i.e., the intraparticle resistance decreases (N_D increases), then the adsorption/desorption efficiency should improve. In fact the time constant for diffusion is proportional to R_0^2.

Table 3 summarizes the parameter values (N_D and N_f) that vary with the particle radius. For all the simulations N_{hw} is kept constant, being equal to 0.25 and 0.33 for the hot and cold half cycles, respectively. Fixed flowrates for each half cycle were used in the simulations, $Q_{hc} = 3.33\times10^{-6}\ m^3/s$ ($\tau = 653$ s with $L = 0.85$ m) and $Q_{cc} = 2.50\times10^{-6}\ m^3/s$ ($\tau = 876$ s), which means that the time cycle is 5.6 h.

Table 3. Parameter values used in the simulations to study the effect of the adsorbent particle radius.

$R_0\ (10^{-4}m)$	$N_{D(hc)}$	$N_{D(cc)}$	$N_{f(hc)}$	$N_{f(hc)}$
1.0	49.02	26.62	2250	1386
1.5	21.78	11.83	1688	1084
2.0	12.25	6.65	1500	904
3.0	5.45	2.96	1125	723

Effect of the Peclet Number, Pe. Figure 4 shows that if the Peclet number decreases, i.e, the axial dispersion increases, the separation obtained is lower.

The axial dispersion, caused by fluid mixing in the interstices between particles, is considered as a

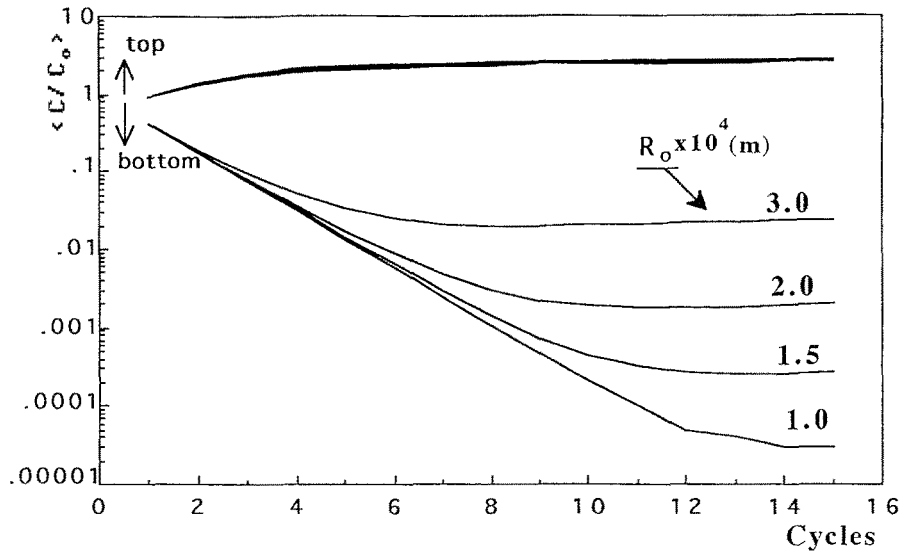

Fig. 3. Effect of the adsorbent particle radius R_0 on top and bottom transient concentrations versus the number of cycles.

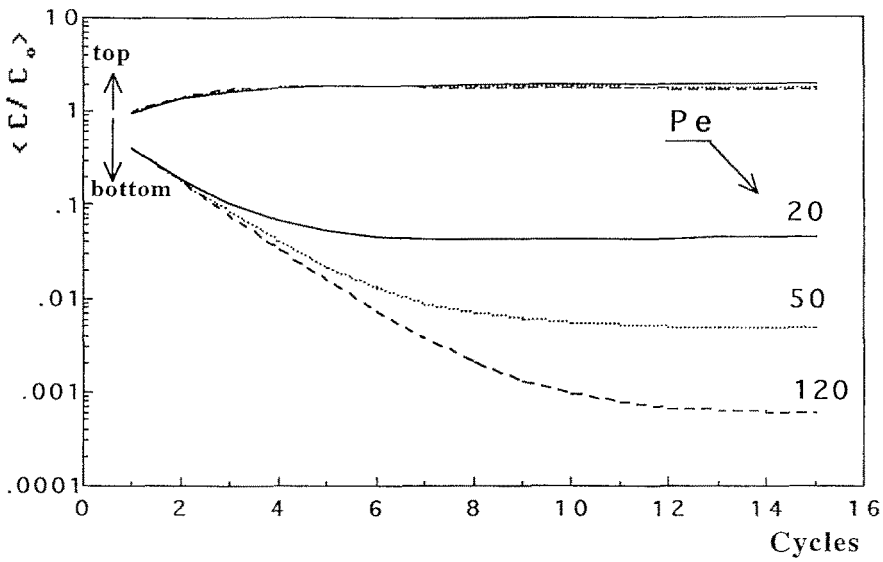

Fig. 4. Effect of the Peclet number Pe, on top and bottom transient concentrations versus the number of cycles.

dispersive effect which tends to limit the separation. It is obvious that if there are no dispersive effects the separation will tend to infinite.

For this case, the parameter values are: $N_D = 7.83$, $N_f = 1158$ and $N_{hw} = 0.22$ for the hot half cycle and $N_D = 4.44$, $N_f = 719$ and $N_{hw} = 0.29$ for the cold half cycle. In all the simulations the cycle time and the fixed bed length were equal to 5.6 h (with $Q_{hc} = 3.33 \times 10^{-6}$ m^3/s and $Q_{cc} = 2.50 \times 10^{-6}$ m^3/s) and 0.75 m, respectively.

Effect of the Dimensionless Dead Volumes, m_1 and m_2. The effect of bottom and top dead volumes are shown in Figs. 5 and 6, respectively. Increasing any of these volumes delays the separation rate but does not affect the ultimate separation. This is expected because m_1 and m_2, as fractions of the volume reservoirs displaced, are not included in the model equations, and are only used to set the boundary conditions. However, concerning the effect of the top dead volume, when this volume is increased less concentrated bottom product

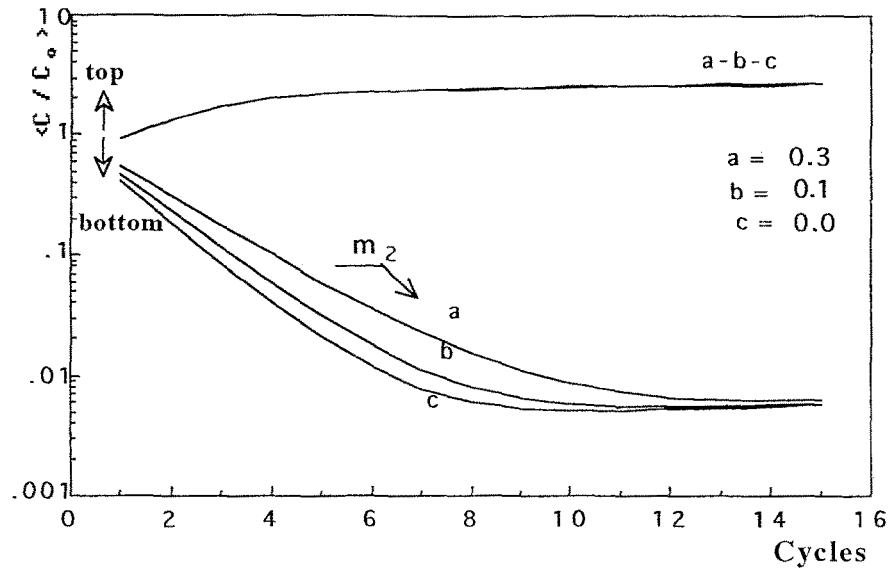

Fig. 5. Effect of the bottom dead volume m_2 on top and bottom transient concentrations versus the number of cycles.

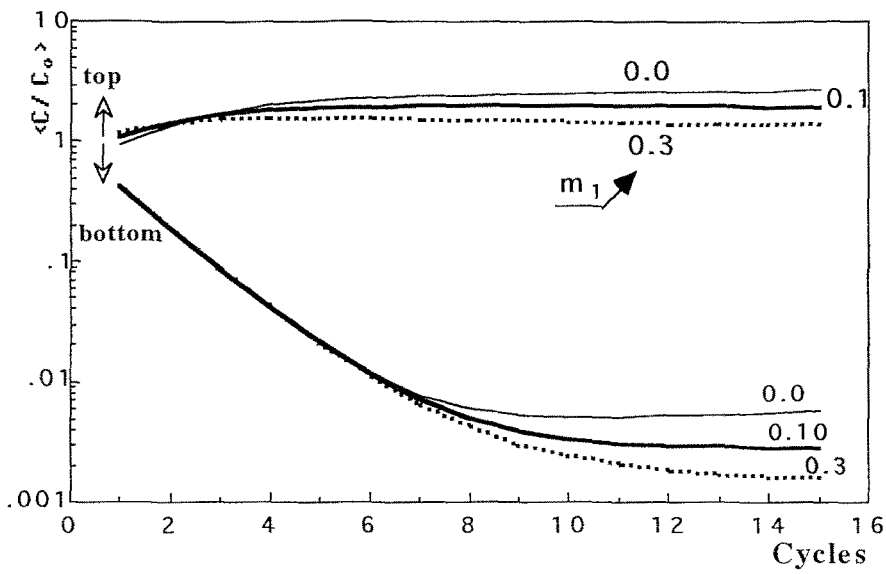

Fig. 6. Effect of the top dead volume m_1 on top and bottom transient concentrations versus the number of cycles.

is produced in the ultimate separation, as is shown in Fig. 6. This should happen because increasing m_1 a more diluted top product goes up into the top reservoir during the hot half cycle; during the cold half cycle that product is pumped in downward flow contributing to the less concentrated solution that enters into the bottom reservoir.

The parameter values used in the simulations are: $N_D = 8.88$, $N_f = 1313$ and $N_{hw} = 0.25$ for the hot half cycle and $N_D = 4.82$, $N_f = 843$ and $N_{hw} = 0.33$ for the cold half cycle. We considered a fixed bed length equal to 0.85 m and the flowrate for each half cycle was kept constant ($t_c = 5.6$ h).

Effect of the Ratio between Fractions of Volume Reservoir Obtained as Bottom and Top Product, ϕ_B/ϕ_T. Increasing ϕ_B/ϕ_T (by increasing ϕ_B) and keeping constant ($\phi_B + \phi_T$), the separation becomes poor, as shown

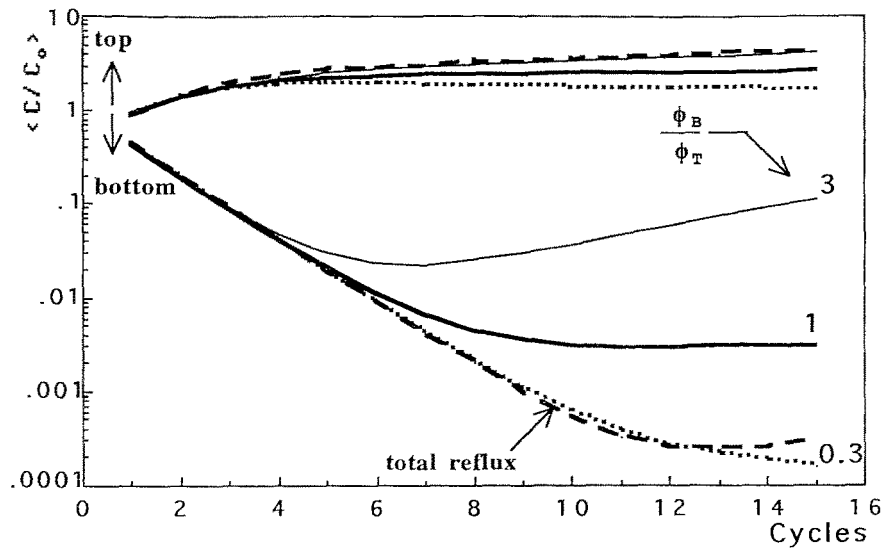

Fig. 7. Effect of the ratio (ϕ_B/ϕ_T) on top and bottom transient concentrations versus the number of cycles.

in Fig. 7. It should be emphasized that when ϕ_B increases more reservoir volume displacement ($Q\pi/\omega$) is percolated during the cold half cycle. In terms of the distance of penetration of the concentration front, one can expect that for larger values of ϕ_B the concentration wave coming from the top penetrates a deeper distance in the column causing more concentrated solution to be obtained as bottom product. Figure 7 also shows that a good separation is obtained in total reflux, when there is neither feed our product streams.

Table 4 shows the parameter values used in each simulation by changing the ratio ϕ_B/ϕ_T. It should be noted that the flowrate for the cold half cycles takes different values depending on the fraction of the volume reservoir obtained as bottom product, ϕ_B. This is so because the cold half cycle time was kept constant ($t_{ch} = 217$ min) when the volume $Q(\pi/\omega)$ percolated downwards changes. Therefore only the parameters $N_{D(cc)}$, $N_{f(cc)}$ and $N_{f(cc)}$ are affected because they depend on the space time τ (inversely proportional to flowrate).

Effect of the Adsorbent Capacity, Q_∞. Figure 8 shows that the separation is strongly dependent on the absorbent capacity Q_∞. For higher adsorbent capacity the separation is improved. The separation is based on the differences in the adsorption equilibrium caused by changing the temperature. Increasing Q_∞, at fixed temperatures (20 and 60°C), leads to larger changes in adsorption and improved separation performance.

Parameter values used in the simulations are: $N_D = 8.88$, $N_f = 1313$ and $N_{hw} = 0.25$ for the hot half cycle and $N_D = 4.82$, $N_f = 843$ and $N_{hw} = 0.33$ for the cold half cycle.

Effect of the Temperature Change, ΔT. Figure 9 shows that better separation is obtained when the temperature is cycled over a wider temperature range (ΔT). For this case, larger changes in equilibrium adsorption occur when the hot temperature increases. The parametric pumping action is based on the solute that is pumped to the top and bottom reservoir when changes in the concentration occur everytime the column temperature is changed. Decreasing the temperature more solute is adsorbed and the fluid concentration decreases. Increasing the temperature the solute is desorbed and the fluid concentration must increase.

The parameter values used in the simulations are: $N_D = 7.83$, $N_f = 1158$ and $N_{hw} = 0.22$ for the hot half cycle and $N_D = 4.44$, $N_f = 719$ and $N_{hw} = 0.29$ for the cold half cycle. A fixed bed length of 0.75 m was used.

The sensitivity of the process performance to changes in operating parameters is summarized in Table 5. The results presented show that is possible to obtain large separation factors for high cycle time (t_c), small ϕ_B/ϕ_T ratio and small particle radius (R_0). For a given system to separate we first screen the adsorbent by looking at adsorption equilibrium isotherm at various temperatures. Once the adsorbent is chosen Q_∞ and ΔT are fixed. The process performance is not very sensitive to bottom and top dead volumes parameters.

Table 4. Parameter values used in the simulations to study the effect of the ratio ϕ_B/ϕ_T.

ϕ_B	ϕ_B/ϕ_T	$Q(\pi/\omega)$ (m^3)	$N_{D(hc)}$	$N_{D(cc)}$	$N_{f(hc)}$	$N_{f(cc)}$	$N_{hw(hc)}$	$N_{hw(cc)}$
0.308	3.0	0.0341	8.88	4.57	1322	783	0.25	0.31
0.205	1.0	0.0297	8.88	5.25	1322	904	0.25	0.36
0.092	0.3	0.0260	8.88	6.00	1322	964	0.25	0.41
0.000	total reflux	0.0236	8.88	6.60	1322	1024	0.25	0.45

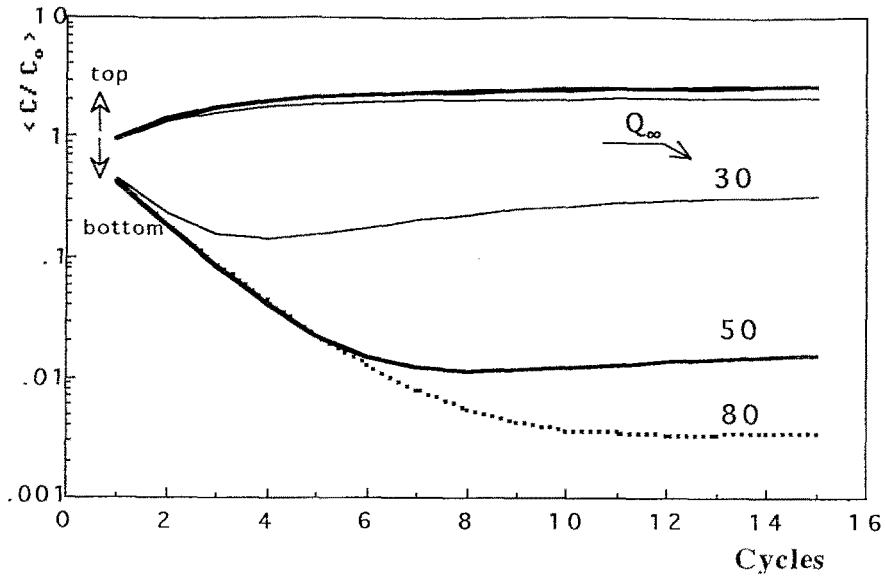

Fig. 8. Effect of the adsorbent capacity Q_∞ on top and bottom transient concentrations versus the number of cycles.

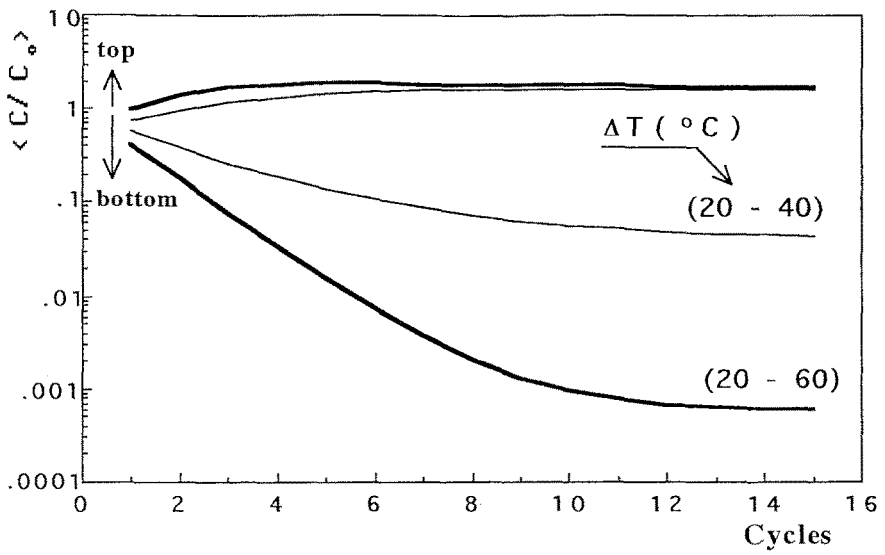

Fig. 9. Effect of the temperature change ΔT on top and bottom transient concentrations versus the number of cycles.

Table 5. Summary of the sensitivity analysis

Parameter	Final reservoir concentration, kg/m^3 (C_0-initial solute concentration = 0.1 kg/m^3) Top (C_{TP})	Bottom ($C_{BP} \times 10^3$)	Separation factor C_{TP}/C_{BP}
Cycle time, t_c (h)			
2.9	0.165	0.595	277
3.5	0.166	0.211	787
4.0	0.163	0.115	1417
6.2	0.168	0.033	5091
Ratio, ϕ_B/ϕ_T			
total reflux	0.428	0.029	14759
0.3	0.171	0.016	10688
1.0	0.261	0.310	842
3.0	0.411	11.36	36
Particle radius, R_0 (10^{-4} m)			
1.0	0.279	0.003	93000
1.5	0.274	0.027	10148
2.0	0.270	0.199	1357
3.0	0.257	2.381	108
Peclet number, Pe			
20	0.197	4.467	44
50	0.179	0.474	378
120	0.169	0.058	2914
Bottom dead volume, m_2			
0	0.266	0.573	464
0.1	0.267	0.584	457
0.3	0.270	0.622	434
Top dead volume, m_1			
0	0.266	0.573	464
0.1	0.191	0.279	685
0.3	0.134	0.152	882
Adsorbent capacity, Q_∞ (kg solute/kg dry resin)			
0.03	0.213	32.1	7
0.05	0.260	1.56	167
0.08	0.271	0.34	797
Temperature change, ΔT (°C)			
20–40	0.163	4.33	38
20–60	0.169	0.058	2914

Evolution of the Histories and Axial Profiles of the Concentration and Temperature

The histories of the temperature and concentration are shown in Figs. 10 and 11. From the analysis of the Fig. 10 we can conclude that temperature transients are fast if compared with the half cycle time. As a first approximation, the equilibrium theory allows us to calculate the average temperature wave velocity ($u_{th} = u_i/[1 + \xi_h]$) and the average concentration wave velocity ($u_{cn} = u_i/[1 + m(T)]$ in which $m(T) = [1 - \varepsilon]\rho_{ap}K(T)/\varepsilon$). The velocity of the thermal wave

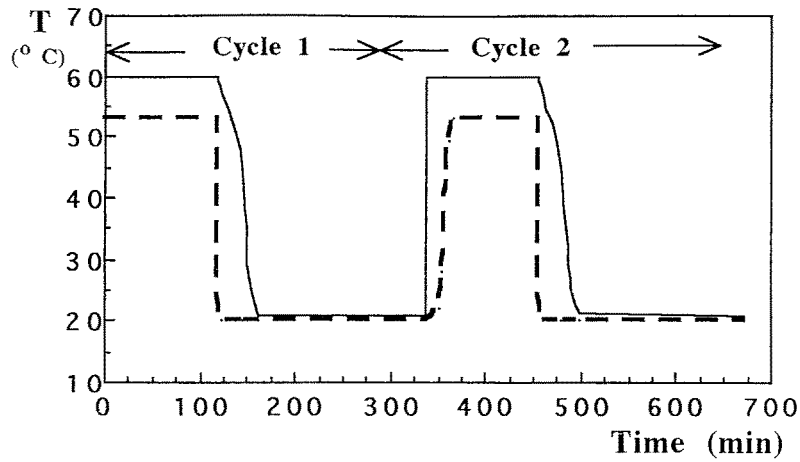

Fig. 10. History of temperatures during the recuperative parametric pumping: bottom temperature (– – –) and top temperature (—).

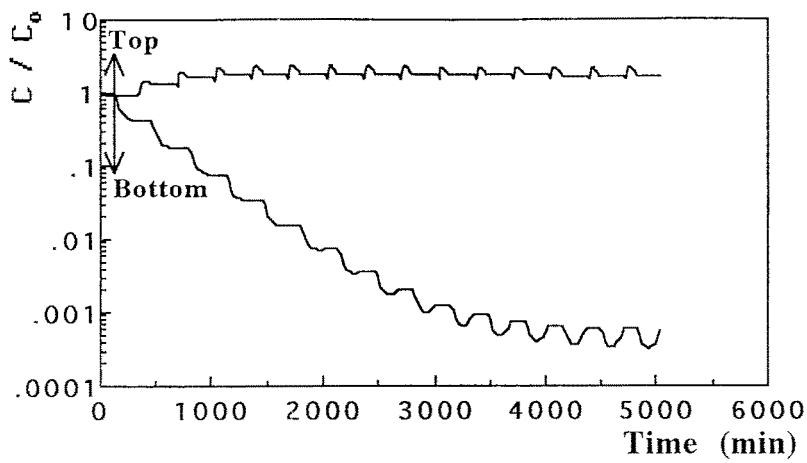

Fig. 11. History of concentrations during the recuperative parametric pumping: top and bottom concentrations versus time.

is practically constant and with $\xi_h = 1.3$ we obtain $u_{th} = 0.435\,u_i$. The fastest concentration wave velocity is observed during the hot half cycle $u_{cn} = 0.094\,u_i$ (with $\varepsilon = 0.4$, $\rho_{ap} = 285$ kg/m^3 and considering a linear isotherm $q^* = K(T)C^*$). This shows that the thermal waves are much faster than the concentration waves and the system behaves close to the direct mode. In Fig. 10, only thermal wave evolution for the first two cycles are shown. The same behavior is repeated for the following cycles.

The behavior of the histories of top and bottom product concentrations, shown in Fig. 11, can be understood by analyzing how the concentration wave travels inside the column, in each half operating cycle. During the hot half cycle, the fixed bed is heated and the solute is desorbed. This causes an increase in the fluid concentration. At the top we collect a product with increasing concentration, as the adsorbent in heated by the thermal wave. After the concentration reaches its maximum value, it decreases due to two factors. The first factor is related to the mixing effect from the addition of solution to the top reservoir with concentration equal to the feed. The second factor is related to the profiles that emerge at the top, which now are less and less concentrated due to the dispersion of the concentration waves coming from the bottom reservoir. In this case, fronts of higher concentration are displaced by lower concentration waves. This factor is less important in the first operating cycles. Concerning the concentration of the bottom product one can observe that it is kept almost constant, since the reservoir contains mixed volumes.

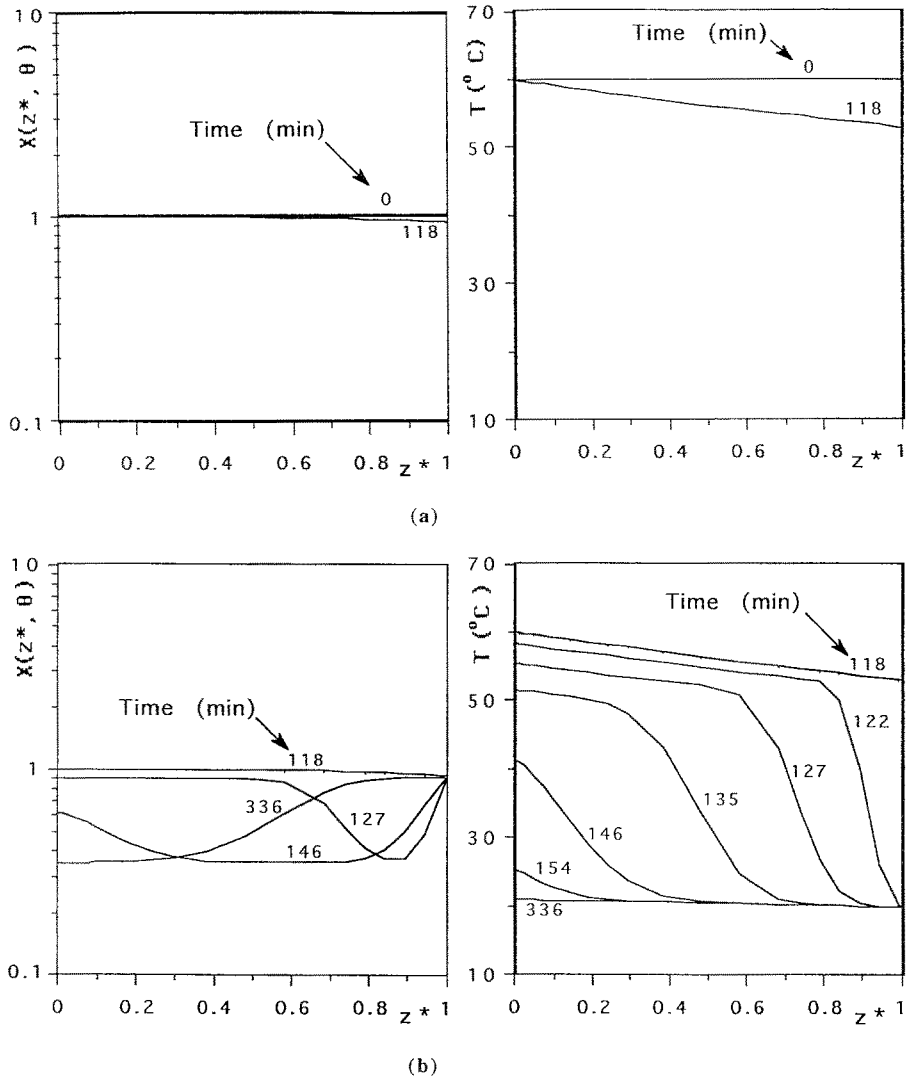

Fig. 12. Concentration and temperature profiles during the first cycle: (a) hot half cycle and (b) cold half cycle.

During the downward flow (cold half cycle), the bed temperature decreases and more solute is adsorbed. This is reflected in a decrease of the fluid phase concentration. As bottom product, we collect a solution of decreasing concentration as the column cools down. The concentration waves that travel in the fixed bed are now compressive. The lower concentration fronts are now displaced by higher concentration waves coming from the top. This effect influences the concentration of the bottom product after 6–7 cycles of operating cycles. The concentration of the top product is uniform during this half cycle when the reservoir feed is interrupted and mixed volumes are considered.

In order to better understand the penetration of the thermal and concentration waves in the bed during each half cycle, and also the process transient evolution as the cycles proceed allowing the collection of more concentrated solution at the top and less concentrated solution at the bottom we follow concentration and temperature profiles in the bed at various times. Figure 12-a shows that during the hot half cycle of the first cycle, the axial profile of concentration at different times is constant because the bed does not undergo a temperature change. At $t = 1$ min, the axial profile of temperature is almost flat when an initial uniform temperature in the bed, $T_0(z^*) = 60°C$, was assumed.

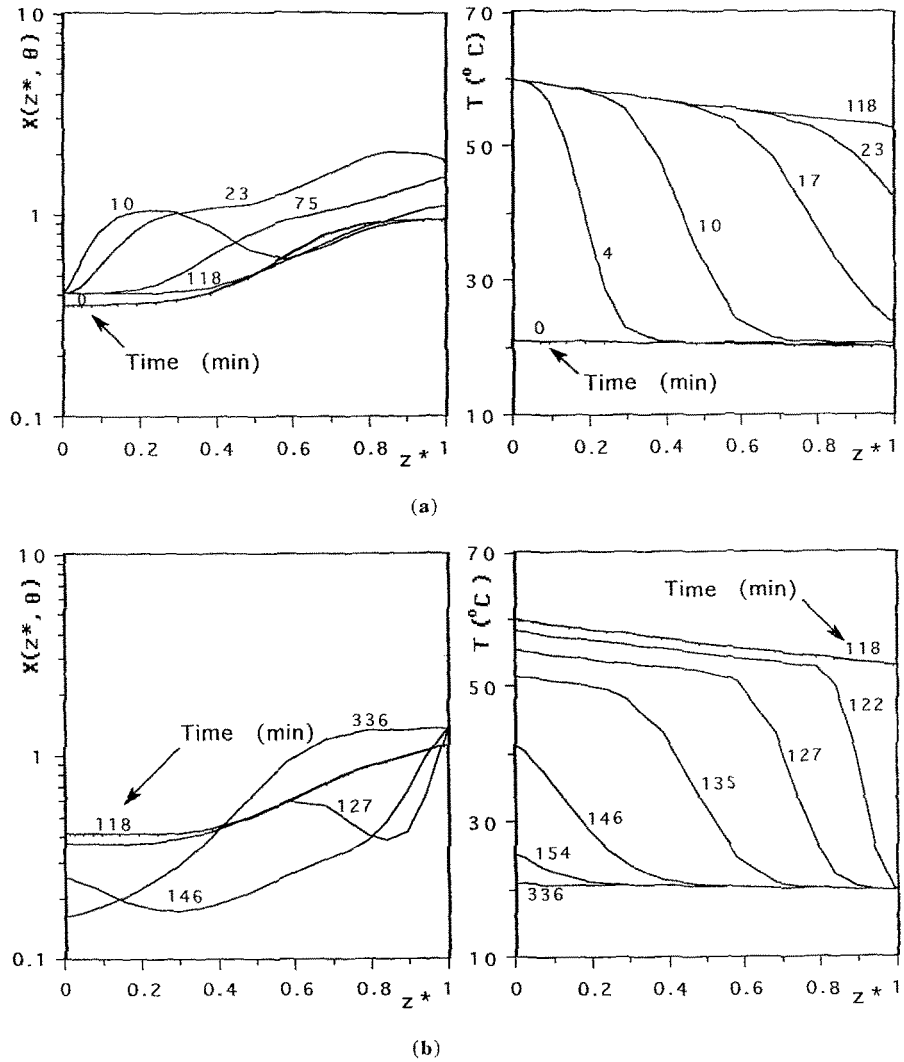

Fig. 13. Concentration and temperature profiles during the 2nd cycle: a) hot half cycle and (b) cold half cycle.

However, a difference of 7–8°C between the temperatures of the top and bottom is found when the system reaches the thermal steady state. This is shown in Fig. 12-a, at the end of 118 minutes.

Figure 12-b shows axial concentration profiles at various times during the cold half cycle of the first cycle. During a short transient period, around 40 minutes, the top thermal wave propagates down the column because cold solution ($T = 20°C$) is fed at $z^* = 1$ in downward flow. So, the temperature inside the bed decreases, the solute is more adsorbed and a decrease in the concentration profile can be observed near the top of the bed ($z^* = 1$) at 127 min. Figure 12-b also shows that the temperature wave travels faster than the concentration wave; in fact at $t = 154$ min the bed is almost completely at 20°C although the concentration front is still near the top of the column. Since at $t = 154$ min the bed is almost completely at 20°C the concentration at the bottom ($z^* = 0$) decreased. From that time on there is propagation of a concentration wave in a bed at 20°C.

Figure 13 shows the concentration and temperature axial profiles during the second hot and cold half cycles. Looking at the concentration axial profile (Fig. 13-a) in the hot half cycle when feed from the bottom ($z^* = 0$) at 60°C enters the column, the solute is desorbed and the concentration profile increases near the bed inlet. However, at $t = 10$ min, 60% of the bed is still at 20°C;

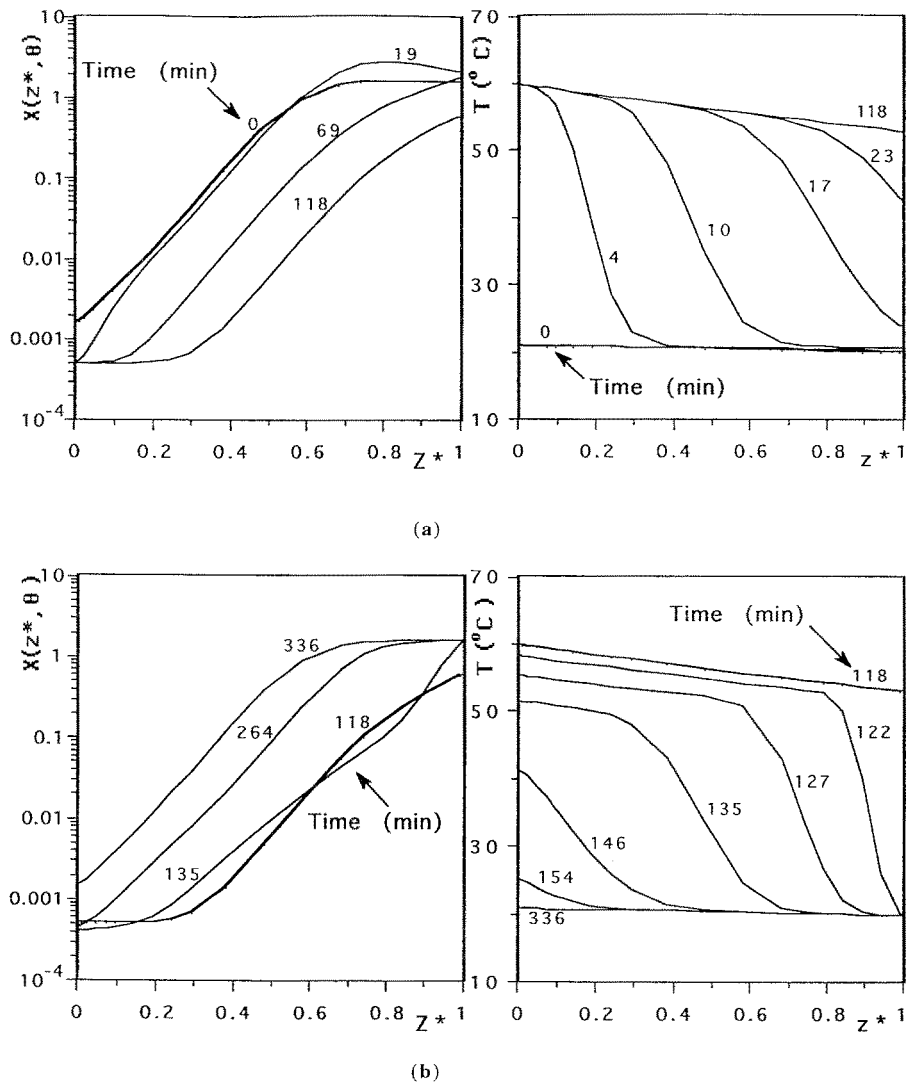

Fig. 14. Concentration and temperature profiles during the 15th cycle: (a) hot half cycle and (b) cold half cycle.

therefore, in that region the concentration profile is the one at the end of cycle 1. In between those regions of the bed there is a maximum in concentration. At $t = 23$ min the bed is almost at 60°C so the concentration wave travels from the bottom to the top; the concentration maximum is now near the top of the column.

After 15 cycles a cyclic steady state is reached. In fact, concentration and temperatures profiles at the end of the cycle 6 are very similar to those at end of cycle 15.

The Process Dynamics at the Cyclic Steady State

In the parametric pumping process cycles are repeated until a cyclic steady state is reached. In a cyclic open system, operating in steady state, each cycle is the repeat of the previous cycle (Lavie, 1972). Steady state solutions for the batch, semi-continuous and continuous systems, based on the equilibrium theory, were presented by Chen and Hill (1971). Features of ultimate separation for batch systems by analyzing frequency responses, were studied in the following works: Rice (1973); Foo and Rice (1975, 1977), Rice (1976) and Rice et al. (1979). Rice and Foo (1981) extended the study to continuous systems. A non equilibrium model to calculate steady state concentrations, for a batch system, was presented by Gupta and Sweed (1973). Steady state characteristic solutions for the continuous recuperative mode, using the equilibrium model, were

developed by Wankat (1978). Pigford et al. (1969) showed that the separation factor for the nth-cycle, when there are no dispersive effects, is given by: $\alpha_n = (2+\frac{2b}{1+b})(\frac{1+b}{1-b})^n - (\frac{1+b}{1-b})^2$, where b is the parameter that reflects the magnitude of the separation as function of two temperatures in the absorption equilibrium.

In the ultimate separation, lim $\alpha_n \rightarrow \infty$; however, in real systems, the existence of the dispersive effects causes a finite ultimate separation.

In our case, around sixteen cycles were needed to obtain the cyclic steady state. The time averaged concentrations in the reservoirs will tend to remain constant, as the operation approaches steady state, since the volume of feed injected at the top reservoir is equal to the sum of solution volumes withdrawn from the top reservoir during upward flow (hot half cycle) and from the bottom reservoir during the downward flow (cold half cycle). This is shown in Fig. 11.

The bed dynamics of the process in 15th-cycle can be seen in Figs. 14 and 15. A higher concentration change occurs in a region close to the ends of the bed, during the beginning of each half cycle, as a consequence of the penetration of the thermal wave and its effect on the adsorption capacity. The development of a solute concentration plateau near the bottom during the hot half cycle and a solute concentration plateau near the top during the cold half cycle, should also be mentioned.

At the cyclic steady state, axial temperatures profiles change almost from hot temperature until cold temperature, since temperature waves propagate faster than concentration waves and half cycles times

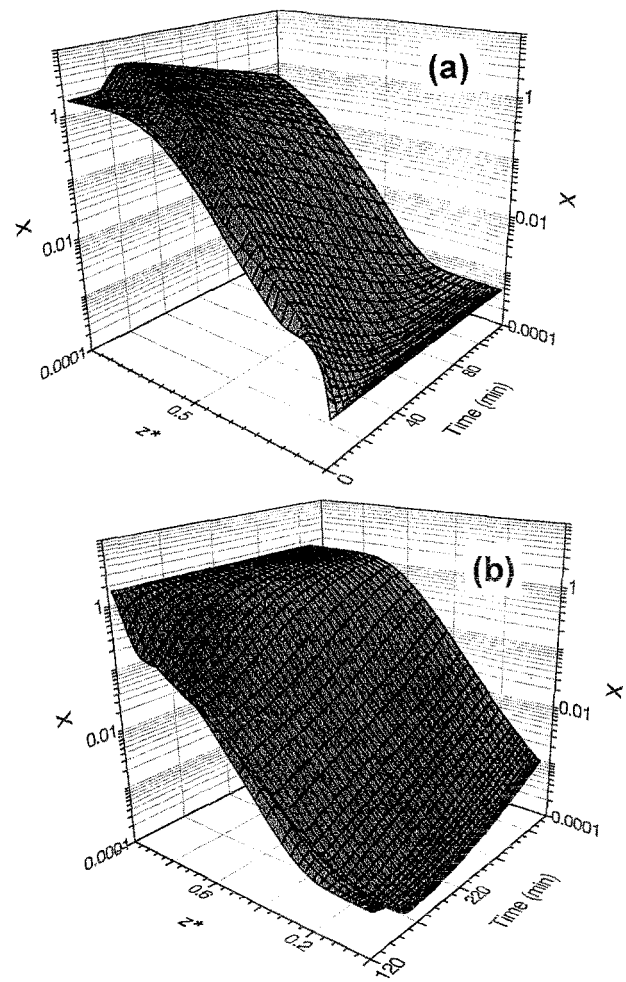

Fig. 15. Bed dynamics at steady state: (a) hot half cycle and (b) cold half cycle.

are longer than the time needed by the temperature wave to travel through the bed. Typically, in a hot half cycle ($t_{hc} = 118$ min), the time that the temperature wave takes to pass through the bed is 40 min. Therefore one can think at this process as a direct mode parametric pumping during 2/3 of cycle time.

The axial concentration profiles at cyclic steady state are kept between 2 extremes profiles in each half cycle; concentration waves move in that bed region.

Conclusions

A detailed model taking into account dispersive effects (intraparticle mass transfer resistance, film mass transfer, axial dispersion for mass and heat), wall heat transfer and nonlinear adsorption equilibrium was developed to study the dynamics of the semicontinuous recuperative parametric pumping process. We have explored the effect of certain operating variables on the sensitivity of the process performance. For a given separation system the absorbent is chosen based on adsorption capacity and temperature change ΔT which requires the measurement of adsorption isotherms at various temperatures. The separation is very sensitive to cycle time (by changing the flowrate), ϕ_B/ϕ_T ratio and particle size. Long cycle times and small ϕ_B/ϕ_T ratios improve the process performance. The separation is not very sensitive to bottom and top dead volumes. The sensitivity results indicate the range of parameters leading to optimal conditions to purify aqueous phenolic solutions.

The transient evolution of the bottom and top concentrations from the initial conditions to the cyclic steady state was better analyzed by looking at the dynamics inside the bed. Operating with a cycle time equal to 5.6 h, we needed around fifteen cycles ($\approx$ four days) to reach the cyclic steady state; the bottom concentration was now about $0.001C_0$.

Finally, the present study served as the basis for the design of parametric pumping experiments in an automated pilot plant. In part II, the complete model is used to simulate the experimental parametric pumping behavior.

It should be stressed that simulations were based on a purification system for phenol-water/Duolite ES 861 since basic data were available on such system at small scale parametric pumping. However, we believe that parametric pumping is more interesting for low volume separation of valuable products (e.g., aminoacids separations).

Nomenclature

$a_i(z^*, \theta)$	coefficients of the trial solution
a_w	specific area of wall, m^{-1}
b	separation parameter
C	solute concentration in the fluid phase, kg/m^3
C_E	initial (feed) solute concentration, kg/m^3
c_{pf}	heat capacity of the fluid, kJ/(kg.K)
C_p	solute concentration in the pores, kg/m^3
c_s	heat capacity of the adsorbent, kJ/(kg.K)
d	column diameter, m
D_{ax}	axial dispersion coefficient, m^2/s
D_m	molecular diffusion coefficient, m^2/s
D_P	pore diffusivity, m^2/s
d_p	particle diameter, m
f_H	humidity factor for the adsorbent (kg dry resin/kg wet resin)
G_f	fluid mass flowrate, $kg/(m^2.s)$
h_k	length of subinterval k
h_{we}	wall heat transfer coefficient, $kJ/(m^2.s.K)$
$(-\Delta H)$	heat of adsorption, kJ/kgmol
$H_i(g_k)$	Hermite polynomials over the subinterval k
j_D	Chilton-Colburn factor
$K(T)$	slope of linear isotherm
K_{ae}	axial thermal conductivity, kJ/(m.s.K)
K_f	film mass transfer coefficient, m/s
K_L	parameter of the Langmuir isotherm, m^3 solution /kg solute
k_0	parameter of the modified Langmuir isotherm, m^3 solution /kg solute
L	bed height, m
$m(T)$	mass capacity parameter
n	number of cycles
N_D	number of mass transfer units for pore diffusion
N_f	number of film mass transfer units
N_{hw}	number of wall heat transfer units
Pe	mass Peclet number
Pe_h	thermal Peclet number
q	adsorbed solute concentration, kg solute /kg dry resin
Q	flowrate in the column, m^3/s
Q_{hc}	flowrate in the hot half cycle, m^3/s
Q_{cc}	flowrate in the cold half cycle, m^3/s
Q_∞	maximum adsorbent capacity, kg solute /kg dry resin
$(Q\pi/w)$	reservoir displacement volume, m^3
r	radial coordinate, m
R	ideal gas constant, kJ/(kgmol.K)
R_0	particle radius, m

Re	particle Reynolds number
Sc	Schmidt number
Sh	Sherwood number
t	time, s
t_c	cycle time, s
t_{cc}	cold half cycle time, s
t_{hc}	hot half cycle time, s
T	temperature, K
T_a	ambient temperature, K
T_{cc}	cold temperature, K
T_{hc}	hot temperature, K
u	superficial velocity, m/s
u_{cn}	concentration wave velocity, m/s
u_i	interstitial velocity, m/s
u_{th}	thermal wave velocity, m/s
u^*	normalized radial coordinate
u_k^*	inferior limit of subinterval k
u_{k+1}^*	upper limit of subinterval k
V_U	volume percolated in upward flow, m^3
X	normalized fluid phase concentration
X_p	normalized fluid concentration in the pores
z	spatial coordinate, m
z^*	normalized axial coordinate
$\langle\ \rangle$	average value

Greek Letters

ξ_h	thermal capacity parameter
ε	bed porosity
ε_p	intraparticle porosity
ϕ_B, ϕ_T	fractions of the $Q\pi/\omega$ that are withdrawn as bottom and top products, respectively
ν	kinematics viscosity, m^2/s
ρ_{ap}	apparent density of the adsorbent, kg/m^3
ρ_f	density of the fluid, kg/m^3
ρ_s	density of the adsorbent, kg/m^3
ρ_h	wet density of the adsorbent, kg/m^3
θ	normalized time
ω	frequency of temperature change
τ	space time, s
τ_p	tortuosity factor
π/ω	duration of half cycle

Subscripts

E	entrance
BP	bottom product
cc	cold half cycle
hc	hot half cycle
0	initial
TP	top product

Acknowledgment

Financial support from the Commission of the European Communities—EEC (Project EV4V-0072-C(TT)) and JNICT is gratefully acknowledged.

References

Apostolopoulos, G.P., "The Parametric Pumping as a Chemical Reactor," *Ind. Eng. Chem. Fundam.*, **14**, 11–16 (1975).

Apostolopoulos, G.P., "The Parametric Pumping as a Chemical Reactor," *Ind. Eng. Chem. Fundam.*, **15**, 14 (1976).

Chen, H.T. and F.B. Hill, "Characteristics of Batch, Semicontinuous and Continuous Equilibrium Parametric Pumps," *Separation Science*, **6**, 411–434 (1971).

Chen, H.T., J.L. Rak, J.D. Stokes, and F.B. Hill, "Separation Via Semicontinuous Parametric Pumping," *AIChE J.*, **18**, 356–361 (1972).

Chen, H.T., J. Reiss, J.J. Stokes, and F. Hill, "Separation Via Continuous Parametric Pumping," *AIChE J.*, **19**, 589–595 (1973).

Chen, H.T., T.K. Hsieh, H.C. Lee, and F.B. Hill, "Separation of Proteins Via Semicontinuous pH Parametric Pumping," *AIChE J.*, **23**(5), 695–701 (1977).

Chen, H.T., Y.W. Wong, and S. Wu, "Separation of Proteins Via Multicolumn pH Parametric Pumping," *AIChE J.*, **26**(5), 839–849 (1980).

Chen, H.T., W.T. Yang, U. Pancharoen, and R. Parisi, "Continuous Fractionation of Protein Mistures by pH Parametric Pumping," *AIChE J.*, **25**(2), 320–327 (1979).

Costa, C., A. Rodrigues, G. Grevillot, and D. Tondeur, "Purification of Phenolic Wastewater by Parametric Pumping: Non Mixed Dead Volume Equilibrium Model," *AIChE J.*, **28**(1), 73–85 (1982).

Costa, C. and A. Rodrigues, "Design of Cyclic Fixed Bed Adsorption Processes. Part I: Phenol Adsorption on Polymeric Adsorbents," *AIChE J.*, **3**(1), 1645–1654 (1985).

Ferreira, L.M., "Dynamics of Sorption Processes: Separation by Parametric Pumping and Recovery of Metals with Complexing Resins," Ph.D. Thesis, University of Porto, Portugal (1994).

Finlayson, B.A., *Non-linear Analysis in Chemical Engineering*, McGraw-Hill Int., New York, 1980.

Foo, S.C. and R.G. Rice, "On The Prediction of Ultimate Separation in Parametric Pumps," *AIChE J.*, **21**, 1149–1158 (1975).

Foo, S.C. and R.G. Rice, "Steady State Predictions for Nonequilibrium Parametric Pumps," *AIChE J.*, **23**, 120–125 (1977).

Gregory, R.A. and N.H. Sweed, "Parametric Pumping Behavior of Open Systems Part I: Analytical Solutions," *The Chem. Eng. J.*, **1**, 207–216 (1970).

Grevillot, G. and D. Tondeur, "Equilibrium Staged Parametric Pumping I—Single Transfer Step per Half-Cycle and Total Reflux—the Analogy with Distillation," *AIChE J.*, **22**, 1055–1063 (1976).

Grevillot, G. and D. Tondeur, "Equilibrium Staged Parametric Pumping II—Multiple Transfer Steps per Half-Cycle and Reservoir Staging," *AIChE J.*, **23**, 840–851 (1977).

Grevillot, G., "Equilibrium Staged Parametric Pumping Part III. Open Systems at Steady-State-McCabe-Thiele Diagrams," *AIChE J.*, **26**, 120–131 (1980).

Gupta, R. and N.H. Sweed, "Modeling of Nonequilibrium Effects in Parametric Pumping," *Ind. Eng. Chem. Fundam.*, **12**, 335–341 (1973).

Hollein, H.C., H.-C. Ma, C.-R. Huang, and H.T. Chen, "Parametric Pumping with pH and Electric Field: Protein Separations," *Ind. Eng. Chem. Fundam.*, **12**, 205–214 (1982).

Lavie, R. and M.J. Reilly, "Limit Cycles in Fixed Beds Operation in Alternating modes," *Chem. Engng. Sci.*, **27**, 1835–1843 (1972).

Madsen, N.K. and R.F. Sincovec, "PDECOL: General Collocation Software for Partial Differential Equations," *ACM Trans. Math. Software*, **3**, 326–351 (1979).

Pigford, R., B. Baker, and D. Blum, "An Equilibrium Theory of the Parametric Pump," *Ind. Eng. Chem. Fundam.*, **8**, 144–149 (1969).

Rice, R.G., "Dispersion and Ultimate Separation," *Ind. Eng. Chem. Fundam.*, **12**, 406–412 (1973).

Rice, R.G., "Progress in Parametric Pumping, Separation and Purification Methods," **5**, 139–188 (1976).

Rice, R.G. and S.C. Foo, and G.G. Gough, "Limiting Separation in Parametric Pumps," *Ind. Eng. Chem. Fundam.*, **18**, 117–123 (1979).

Rice, R.G. and S.C. Foo, "Continuous Desalination Using Cyclic Mass Transfer on Bifunctional Resins," *Ind. Eng. Chem. Fundam.*, **20**, 150–155 (1981).

Sweed, N.H. and R.H. Wilhelm, "Parametric Pumping Separations via Direct Thermal Mode," *Ind. Eng. Chem. Fundam.*, **8**, 221–231 (1969).

Sweed, N.H. and R.A. Gregory, "Parametric Pumping: Modeling Direct Thermal Separations of Sodium Chloride-Water in Open and Closed Systems," *AIChE J.*, **17**, 171–176 (1971).

Wankat, P.C. "Continuous Recuperative Mode Parametric Pumping," *Ind. Eng. Chem. Fundam.*, **12**, 372–380 (1973).

Wankat, P.C. "Liquid-Liquid Extraction Parametric Pumping," *Chem. Engng. Sci.*, **33**, 723–733 (1978).

Wilhelm, R.H., A.W. Rice, and A.R. Bendelius, "Parametric Pumping: A Dynamic Principle for Separation Fluid Mixtures," *Ind. Eng. Chem. Fundam.*, **5**, 141–144 (1966).

Wilhelm, R.H., A.W. Rice, R.W. Rolke, and N.H. Sweed, "A Dynamic Principle for Separation Fluid Mixtures," *Ind. Eng. Chem. Fundam.*, **7**, 337–348 (1968).